

Waveform Design for 4D-Imaging mmWave PMCW MIMO Radars with Spectrum Compatibility

Nazila Karimian Sichani[#], Mohammad Alae-Kerahroodi^{*}, Bhavani Shankar^{*},
Esfandiar Mehrshahi[#], Seyyed Ali Ghorashi^{##}

[#]Department of Telecommunications, Faculty of Electrical Engineering, Shahid Beheshti University, Tehran 1983963113, Iran.

^{*}Interdisciplinary Centre for Security, Reliability and Trust (SnT), University of Luxembourg, Luxembourg.

^{##}Department of Computer Science and Digital Technologies, School of Architecture, Computing and Engineering, University of East London, E16 2RD, London, UK.

Abstract—4D-imaging mmWave radars offer high angular resolution in both azimuth and elevation, but achieving this requires a large antenna aperture size and a significant number of transmit and/or receive channels. This presents a challenge for designing transmit waveforms that are both orthogonal and separable on the receive side, as well as having low auto-correlation sidelobes. This paper focuses on designing an orthogonal set of sequences for 4D-imaging radar sensors based on PMCW technology. We propose an iterative optimization framework based on Coordinate Descent, which considers the Regions Of Interest (ROI) and optimizes a phase-modulated constant modulus waveform set based on weighted integrated sidelobe level on the required ROI and spectrum shaping. The optimization also accounts for the radar working adjacent to communication systems and other radar sensors. Simulation results are provided to demonstrate the effectiveness of the proposed method, which achieves low sidelobe levels and is compatible with spectrum constraints.

Keywords—mmWave Radar, PMCW, CDM-MIMO, WISL, Waveform design, Spectrum shaping.

I. INTRODUCTION

High resolution 4D-Imaging millimeter-Wave (mmWave) Multiple-Input Multiple-Output (MIMO) radars, are being widely employed in various applications including indoor sensing, health care, and autonomous driving [1]. To achieve high azimuth-elevation angular resolution in these sensors, a large antenna aperture size and a large number of transmit/receive channels are necessary. However, these requirements can be fulfilled virtually by utilizing sparsity in the location of transmit or receive antenna elements. This improved angular resolution capabilities of 4D-imaging mmWave MIMO radars come with a cost of increased complexity in designing transmit waveforms, as orthogonality in transmission is required, which necessitates a multiplexing scheme. In mmWave radar sensors, Frequency-Modulated Continuous-Wave (FMCW) waveforms have traditionally been favored due to their cost-effective implementation using de-chirp techniques and low sampling rate ADCs [2]. However, in MIMO applications where a set of orthogonal waveforms is required to be transmitted, the interest has shifted towards using Code-Division Multiplexing (CDM) techniques where potentially Phase-Modulated Continuous-Wave (PMCW) can be transmitted [3]–[6]. The reason is that, Time-Division Multiplexing (TDM) [7]–[9] and Frequency Division Multiplexing (FDM) [10] multiplexing of FMCW do

not make full use of available time and frequency resources, and BPM [11], [12] and Doppler-Division Multiplexing (DDM) [13], [14] create folding in the useful Doppler region. PMCW waveforms offer greater adaptability to environmental conditions and hold the potential for enabling cognition with capability of spectrum sharing [15], making them an attractive alternative to FMCW, provided that the orthogonality between transmitting waveforms is guaranteed [3]–[6].

Several approaches are available in the literature to design a set of sequences with small auto- and cross-correlation sidelobes for PMCW radars based on the Integrated Side-lobe Level (ISL)/Weighted Integrated Side-lobe Level (WISL) or Peak Side-lobe Level (PSL) metrics, including Multi-Cyclic Algorithm New (CAN) [16], Iterative Direct Search [17], ISLNew [18], Majorization-Minimization (MM)-Corr, [19] and Coordinate Descent (CD) [6], [20], [21]. Furthermore, it is possible to design the waveforms for mmWave radars compatible with other transmissions operating in the same frequency range. This is achieved by incorporating spectral shaping methods into the optimization process for the sequence set. Thus, the waveforms can have minimal interference with other transmissions in the frequency band [22]–[26]. The contributions of this paper are summarized as follows; An unconstrained optimization problem is formulated to design a set of spectrally compatible sequences with very low range-sidelobe levels (good orthogonality) in a ROI realized by the WISL metric and a weight vector for spectrum shaping. An entry-based CD approach is then proposed to tackle the problem for the continuous-phase constraint. In each step, the global solution is obtained leading to a monotonically decreasing objective function until a convergence criteria is met. Finally, numerical results validate the proposed algorithm's performance for mmWave 4D-imaging radars¹.

II. WAVEFORM OPTIMIZATION

In this section, we design a set of unimodular sequences for PMCW radars based on jointly minimizing their auto- and cross-correlation sidelobe levels and shaping their spectrum.

¹**Notation:** We use boldface upper case \mathbf{X} for matrices and boldface lower case \mathbf{x} for vectors. The $(m, n)^{th}$ element of \mathbf{X} is denoted by $\mathbf{X}_{m,n}$. The sets of complex number, real number, Hadamard product, l_2 norm, phase of vector and matrix, hermitian operation, Transpose operation, modulus of the complex number, correlation, and gradient are denoted by, \mathbb{C}^N , \mathbb{R}^N , \odot , \angle , $\|\cdot\|_2$, \angle , $(\cdot)^H$, $(\cdot)^T$, $|\cdot|$, \otimes , and ∇ respectively. \ln defines the natural logarithm.

The aim is to reduce the sidelobes as much as possible in a ROI, which can be calculated based on the radar system's maximum range. Let us assume that $\mathbf{X} \in \mathbb{C}^{M \times K}$ is the set of sequences in baseband with M transmit antennas and K samples for each, and $x_{m,k} = e^{j\phi_{m,k}}$ is the k^{th} sample of m^{th} antenna. WISL metric is defined by:

$$\sum_{m=1}^M \sum_{l=1}^M \sum_{k'=-K+1}^{K-1} |\alpha_{m,l}(k') r_{m,l}(k')|^2 - \sum_{m=1}^M |\alpha_{m,m}(0)K|^2 \quad (1)$$

where $\alpha_{m,l}(k') \in [0, 1]$, $\forall k' \in \{-K+1, \dots, K-1\}$ represents a set of weights, $r_{m,l}(k') \triangleq (\mathbf{x}_m \circledast \mathbf{x}_l)_{k'} = \sum_{k'=1}^{K-1} x_{m,k'} x_{l,K-k'}^*$ is the cross-correlation between m^{th} and l^{th} antenna waveforms, that are $\mathbf{x}_m = [x_{m,1}, x_{m,2}, \dots, x_{m,K}]^T$ and $\mathbf{x}_l = [x_{l,1}, x_{l,2}, \dots, x_{l,K}]^T$, $m, l \in \{1, 2, \dots, M\}$. If $m = l$, $r_{m,l}(\cdot)$ represents the auto-correlation of the m^{th} signal. k' is one of the different $(2K-1)$ lags in cross-correlation function. $\sum_{m=1}^M |\alpha_{m,m}(0)K|^2$ is the weighted energy of the waveform. Since the signals are constant modulus, this term is a constant and can be eliminated in the objective function. Re-writing the metric in the frequency domain, we define the following optimization problem:

$$\begin{cases} \min_{\mathbf{X}} & f(\mathbf{X}) \triangleq \sum_{m=1}^M \sum_{l=1}^M \|\mathbf{a}_1 \odot \mathbf{F}^{-1}(\mathbf{a}_2 \odot \mathbf{F}\bar{\mathbf{x}}_m \odot \mathbf{F}\mathbf{x}_l^*)\|_2^2 \\ \text{s.t.} & x_{m,k} \in \mathcal{X}_\infty \end{cases} \quad (2)$$

where, \mathbf{a}_1 and \mathbf{a}_2 are WISL and spectral weight vectors, respectively. $\mathcal{X}_\infty = \{e^{j\phi} | \phi \in \Omega_\infty\}$, $\Omega_\infty \triangleq (-\pi, \pi]$ indicates the unimodular phases. \mathbf{F} and \mathbf{F}^{-1} are $(2K-1)$ points Discrete Fourier Transform (DFT) and Inverse DFT matrices, respectively. $\bar{\mathbf{x}}$, here, is a zero-padding operation, i.e., $\bar{\mathbf{x}}_m \triangleq [\mathbf{x}_m^T, \mathbf{0}_{K-1 \times 1}^T]^T$ is the zero-padded vector of the m^{th} transmitting waveform. $\mathbf{x}_l^* \triangleq [x_{l,K}^*, x_{l,K-1}^*, \dots, x_{l,1}^*]^T$ is the l^{th} antenna sequence reverse. Since the constraint is an affine set, the related optimization problem is non-convex, multi-variable and NP-hard.

To solve the problem under continuous-phase constraint, we use a CD approach and define an entry-based optimization framework to formulate the problem in terms of each single-variable. This leads to find the critical points and obtains the global optimum solution in each step. To this end, we consider each entry of \mathbf{X} as the only variable to our problem, while keeping the others fixed. Let $x_{m_0, k_0}^{(i)}$ ($m_0 \in \{1, 2, \dots, M\}$ and $k_0 \in \{1, 2, \dots, K\}$) be the only entry variable to be optimized in the i^{th} iteration. Storing other entries of \mathbf{X} in $\mathbf{X}_{-(m_0, k_0)}^i$ fixed, we can formulate the objective function ($f(\mathbf{X})$) in terms of x_{m_0, k_0}^i as (for notation simplicity, we omit the iteration number in the equations below):

$$f(x_{m_0, k_0}, \mathbf{X}_{-(m_0, k_0)}) = \nu_{-2}(\mathbf{X}) x_{m_0, k_0}^{*2} + \nu_{-1}(\mathbf{X}) x_{m_0, k_0}^* + \nu_0(\mathbf{X}) + \nu_1(\mathbf{X}) x_{m_0, k_0} + \nu_2(\mathbf{X}) x_{m_0, k_0}^2 \quad (3)$$

where the coefficients ν_{-2} , ν_{-1} , ν_0 , ν_1 and ν_2 are the complex-valued functions of \mathbf{X} having different values for each entry (m_0, k_0) and can be calculated from Table 1, where \mathbf{f}_{k_0} is a vector derived from \mathbf{F} containing its k_0^{th} column elements. Similarly, \mathbf{f}_{K+1-k_0} is the $(K+1-k_0)^{\text{th}}$ column of \mathbf{F} . $\hat{\mathbf{F}}_{-k_0}$ is a $((2K-1) \times K)$ sub-matrix of \mathbf{F} containing all first

K columns of \mathbf{F} , except for the k_0^{th} column, i.e., in $\hat{\mathbf{F}}_{-k_0}$, the k_0^{th} column of (\mathbf{F}) is omitted. The same as $\hat{\mathbf{F}}_{-k_0}$, $\hat{\mathbf{F}}_{-K+1-k_0}$ is a sub-matrix of \mathbf{F} in which the $(K+1-k_0)^{\text{th}}$ column is removed. Also, $\mathbf{x}_{m_0, k \neq k_0}$ is the m_0^{th} row of \mathbf{X} , in which the k_0^{th} sample is dropped out and x_{m_0, k_0} is the k_0^{th} sample of m_0^{th} antenna waveform ($m \in \{1, 2, \dots, M\}$). To simplify the notations in Table 1, we define some auxiliary variables as,

$$\begin{cases} \Upsilon_0 \triangleq \mathbf{a}_1^T \odot \mathbf{F}^{-1}(\mathbf{a}_2^T \odot \mathbf{f}_{k_0} \odot \mathbf{f}_{K+1-k_0}), \\ \Upsilon_1(\hat{m}) \triangleq \mathbf{a}_1^T \odot \mathbf{F}^{-1}(\mathbf{a}_2^T \odot \hat{\mathbf{F}}_{-k_0} \mathbf{x}_{\hat{m}, k \neq k_0}^T \odot \mathbf{f}_{K+1-k_0}), \\ \Upsilon_2(\hat{m}) \triangleq \mathbf{a}_1^T \odot \mathbf{F}^{-1}(\mathbf{a}_2^T \odot \mathbf{f}_{k_0} \odot \hat{\mathbf{F}}_{-K+1-k_0} \mathbf{x}_{\hat{m}, k \neq k_0}^H), \\ \Upsilon_3(\hat{m}, \bar{m}) \triangleq \mathbf{a}_1^T \odot \mathbf{F}^{-1}(\mathbf{a}_2^T \odot \hat{\mathbf{F}}_{-k_0} \mathbf{x}_{\hat{m}, k \neq k_0}^T \odot \hat{\mathbf{F}}_{-K+1-k_0} \mathbf{x}_{\bar{m}, k \neq k_0}^H). \end{cases} \quad (4)$$

where all of these variables are vectors of length $(2K-1)$. Note that, since $f(\mathbf{X})$ in Eq. 2 is real-valued, it can be easily proved that $\nu_{-2} = \nu_2^*$ and $\nu_{-1} = \nu_1^*$. Considering the coefficients as $\nu_h(\mathbf{X})$, $h \in \{-2, -1, 0, 1, 2\}$, the above equation based on the phases of each entry ϕ_{m_0, k_0} and the phase matrix $\Phi_{-(m_0, k_0)}$, can be re-written as:

$$f(\phi_{m_0, k_0}, \Phi_{-(m_0, k_0)}) = \sum_{h=-2}^2 \nu_h(\Phi) e^{jh\phi_{m_0, k_0}} \quad (5)$$

To minimize the objective function over Ω_∞ on each entry ϕ_{m_0, k_0} , and as f are differentiable functions for $\phi \in \Omega_\infty$, we can find the solution of $\frac{df(\phi)}{d\phi} = \frac{d \sum_{h=-2}^2 \nu_h e^{jh\phi}}{d\phi} = 0$. In this regard, the derivative of $f(\phi)$ can be obtained by:

$$f'(\phi) = \sum_{h=-2}^2 jh\nu_h e^{jh\phi_{m_0, k_0}} \quad (6)$$

Finding the roots of $f'(\phi)$ in Eq. 6 is equivalent to find the roots of the 4 degree polynomial function $\sum_{n=0}^4 \rho_n z^n = 0$ where $z \triangleq e^{j\phi}$, $\rho_4 = 2\nu_2$, $\rho_3 = \nu_1$, $\rho_2 = 0$, $\rho_1 = -\nu_{-1} = -\nu_1^*$ and $\rho_0 = -2\nu_{-2} = -2\nu_2^*$. Assume z_n , $n = \{1, \dots, 4\}$ are the roots of $\sum_{n=0}^4 \rho_n z^n = 0$, the roots of $f'(\phi) = 0$ are then $\phi_n = -j \ln(z_n)$, $n = \{1, \dots, 4\}$. We only admit the real roots for ϕ . Thus, the global optimum solution for ϕ is:

$$\phi_{m_0, k_0}^* = \arg \min_{\phi} \{f(\phi) | \phi \in \{\phi_n, n = \{1, \dots, 4\}, \Im(\phi_n) = 0\}\} \quad (7)$$

Subsequently, the optimum solution is $x_{m_0, k_0}^{*i} = e^{j\phi_{m_0, k_0}^*}$ and the sequence set matrix \mathbf{X}^{*i} in each iteration is updated until the convergence criteria is met. The proposed algorithm is summarized in **Algorithm 1**. Note that, since f in Eq. 5 is a function of $\sin \phi$ and $\cos \phi$, it is periodic, real and differentiable and has at least two extrema, so its derivative has at least two real roots. As a result, the feasibility of Eq. 7 in each iteration is guaranteed and the problem has the optimum solution.

III. SIMULATION AND RESULTS

In this section, we provide simulation results to assess the performance of the proposed algorithm. Table 2 shows the comparison between the ISL values of a set of random-phase sequences with Multi-CAN [16], MM-Corr [19] BiST [4], and the proposed method in this paper when we do not consider ROI ($K_{ROI} = K$). The small difference between the ISL values of a set of random-phase codes and the lower bound is not enough to design a set of orthogonal codes in a massive

Table 1. Calculation of coefficients (ν_0, ν_1, ν_2) in Eq. 3.

ν_0	$\sum_{m \neq m_0}^M [M \ \mathbf{Y}_1(m)\ _2^2 + M \ \mathbf{Y}_2(m)\ _2^2 + \ \mathbf{Y}_3(m, m_0)\ _2^2 + \ \mathbf{Y}_3(m_0, m_0)\ _2^2 + 2M x_{m, k_0} \mathbf{Y}_1^H(m) \mathbf{Y}_0 + 2M x_{m, k_0} \mathbf{Y}_0^H \mathbf{Y}_2(m) + 2 x_{m, k_0} \mathbf{Y}_1^H(m_0) \mathbf{Y}_3(m_0, m) + 2 x_{m, k_0} \mathbf{Y}_3^H(m, m_0) \mathbf{Y}_2(m_0)]$ $+ \sum_{m \neq m_0}^M \sum_{l \neq m_0}^M [2 x_{l, k_0} x_{m, k_0}^* \mathbf{Y}_0^H \mathbf{Y}_3(m, l) + 2 x_{l, k_0} x_{m, k_0} \mathbf{Y}_1^H(m) \mathbf{Y}_2(l) + 2 x_{l, k_0} \mathbf{Y}_1^H(m) \mathbf{Y}_3(m, l) + 2 x_{m, k_0} \mathbf{Y}_3^H(m, l) \mathbf{Y}_2(l) + \ \mathbf{Y}_3(m, m_0)\ _2^2]$ $+ M^2 \ \mathbf{Y}_0\ _2^2 + M \ \mathbf{Y}_1(m_0)\ _2^2 + M \ \mathbf{Y}_2(m_0)\ _2^2 + \ \mathbf{Y}_3(m_0, m_0)\ _2^2 + 2 \mathbf{Y}_0^H \mathbf{Y}_3(m_0, m_0) $
ν_1	$\sum_{m \neq m_0}^M [x_{m, k_0}^* \mathbf{Y}_0^H \mathbf{Y}_3(m, m_0) + x_{m, k_0} \mathbf{Y}_1^H(m_0) \mathbf{Y}_2(m) + \mathbf{Y}_1^H(m_0) \mathbf{Y}_3(m_0, m) + x_{m, k_0} \mathbf{Y}_1^H(m_0) \mathbf{Y}_2(m) + \mathbf{Y}_3^H(m_0, m) \mathbf{Y}_2(m) + x_{m, k_0}^* \mathbf{Y}_3^H(m_0, m) \mathbf{Y}_0]$ $+ \mathbf{Y}_3^H(m_0, m_0) \mathbf{Y}_2(m_0) + \mathbf{Y}_1^H(m_0) \mathbf{Y}_3(m_0, m_0) + M \mathbf{Y}_1^H(m_0) \mathbf{Y}_0 + M \mathbf{Y}_0^H \mathbf{Y}_2(m_0)$
ν_2	$\mathbf{Y}_1^H(m_0) \mathbf{Y}_2(m_0)$

Algorithm 1 Proposed Algorithm

1: **Inputs:** Initialize random feasible set of sequences $\mathbf{X}^{(0)}$, predefined threshold value ϵ , \mathbf{a}_1 and \mathbf{a}_2 weight vectors.
 2: $i \leftarrow 0$;
 3: Compute $f(\mathbf{X}^{(0)})$ from (2);
 4: **for** $i = 0, 1, \dots$ **do**
 5: $i \leftarrow i + 1$
 6: **for** $m_0 = 1, \dots, M$ **do**
 7: **for** $k_0 = 1, \dots, K$ **do**
 8: Calculate ν_1 and ν_2 using Table 1;
 9: $\rho_4 \leftarrow 2\nu_2$, $\rho_3 \leftarrow \nu_1$, $\rho_2 \leftarrow 0$, $\rho_1 \leftarrow -\nu_1^*$, $\rho_0 \leftarrow -2\nu_2^*$;
 10: Find the roots of $\sum_{n=0}^4 \rho_n z^n = 0$;
 11: Computing $\phi_n = -j \ln(z_n)$, $n = \{1, \dots, 4\}$;
 12: Find the solution ϕ_{m_0, k_0}^* to the problem (7);
 13: Update $x_{m_0, k_0}^i = e^{j\phi_{m_0, k_0}^*}$ (Algorithm 1);
 14: $\mathbf{X}^i = \mathbf{X}_{-(m_0, k_0)}^i |_{x_{m_0, k_0} = x_{m_0, k_0}^i}^i$;
 15: **end for**
 16: **end for**
 17: Compute $f(\mathbf{X}^i)$ from (2);
 18: Stop if $[f(\mathbf{X}^i) - f(\mathbf{X}^{i-1})] / \|f(\mathbf{X}^i)\|_F > \epsilon$
 19: **end for**
 20: **Outputs:** $\mathbf{X}^* = \mathbf{X}^i$.

MIMO radar system [27] such as 4D-imaging radars. On the other hand, Table 3 shows the impact of considering ROI in the proposed waveform design approach. This table provides the ISL values for different number of antennas and code lengths and shows that, the proposed method can achieve a very low-sidelobe levels in the required ranges by increasing the ratio $\frac{K}{K_{ROI}}$. Although in the proposed method the sidelobe levels outside of ROI are very high, only the sidelobe levels in the ROI determines the performance of the radar system and we can perfectly use it in, forexample, automotive applications.

To compare the impact of different parameters, Fig. 1 represents the auto-correlation functions for different code lengths, ROI, number of antennas, and considering/not considering the spectrum-nulling. It is evident that with increasing the number of antennas and considering stop-bands the properties of auto-correlation degrade, yet by considering the ROI and increasing the ratio $\frac{K}{K_{ROI}}$, we achieve a very low sidelobe levels, while doing spectrum shaping. Fig. 2a shows the convergence curve of the CD approach for different waveforms, in the proposed Algorithm 1. The figure shows the monotonically decreasing objective values in each example. In Fig. 2b we compare the range profile of the proposed method with FMCW and Golomb sequence at the receive side. The range profile for FMCW signals is the Fast Fourier Transform (FFT) of beat frequency and for PMCW signals is the

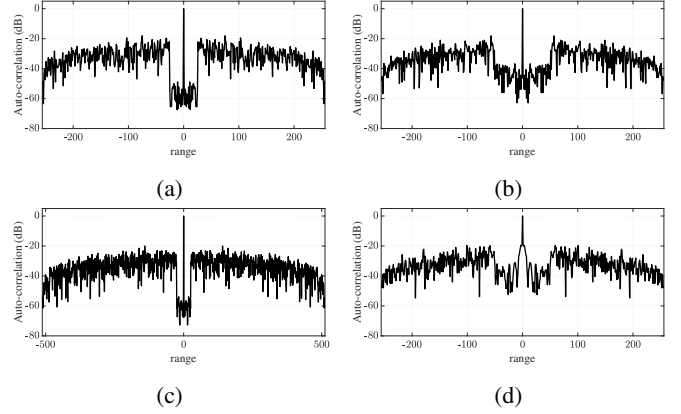


Fig. 1. Auto-correlation functions for (a) $K = 256$, $K_{ROI} = 50$, $M = 2$, and no stop-bands, (b) $K = 256$, $K_{ROI} = 100$, $M = 2$, and no stop-bands, (c) $K = 512$, $K_{ROI} = 50$, $M = 2$, and stop-bands, (d) $K = 256$, $K_{ROI} = 100$, $M = 10$, and stop-bands

matched-filter output. In this example, we set $B = 200$ MHz, $K = 2000$ samples and $R_{max} = 50$ m ($K_{ROI} = 100$ samples). We assume two targets in the range of 15 and 25 m. This figure shows that the proposed method (for $M = 2, 12$, and $M = 12$ with spectrum shaping) have a lower sidelobe levels (in the ROI) while maintaining the same mainlobe width. Also, the chirp signal in FMCW and Golomb sequence, in this figure, are considered to be sent from a single antenna. Hence, in the case of using multiplexing techniques for MIMO FMCW radars or transmitting any other MIMO PMCW sequences lead to a decrease in the performance of radars compared to that of single input FMCW and Golomb sequence in Fig. 2b. For the spectrum compatibility, we consider two scenarios for $K = 128$ and 256 with $K_{ROI} = 50$. To compare the obtained results with [27] in Fig. 2c, we set $m = 2$ and the normalized frequency of stop-bands are $[0.4, 0.5] \cup [0.8, 0.85]$. Although the depth of the obtained nulls is not as good as [27], we achieved better ISL due to the ROI consideration. This figure shows that the proposed method can design a set of spectrally-compatible code sequences with good properties in terms of ISL, while imposing nulls in undesirable stop-bands.

IV. CONCLUSION

In this paper, we considered CDM for MIMO PMCW radars in spectrally crowded environments to design orthogonal

Table 2. Comparison between the ISL (dB)-values of different sequences and random-phase sequences ($K = 64$).

M	2	3	4	5	6	7	8	9	10
Random-phase	5.9289	9.8565	11.9106	14.0384	15.5558	16.8349	18.0590	19.2051	19.9744
Multi-CAN [16]	3.0103	7.7815	10.7918	13.0103	14.7712	16.2325	17.4819	18.5733	19.5424
MM-Corr [19]	3.0103	7.7815	10.7918	13.0103	14.7712	16.2325	17.4819	18.5733	19.5424
BiST [4] ($\theta = 0, L = 8$)	3.2632	7.8529	10.8238	13.0302	14.7901	16.2411	17.4884	18.5796	19.5458
Proposed method ($K_{ROI} = 64, K = 64$)	3.1487	7.8052	10.7975	13.0142	14.7773	16.2346	17.4837	18.5745	19.5433
Lower bound	3.0103	7.7815	10.7918	13.0103	14.7712	16.2325	17.4819	18.5733	19.5424

Table 3. Comparison between the ISL (dB)-values of the proposed method for different code lengths ($K_{ROI} = 64$).

M	2	3	4	5	6	7	8	9	10
$K = 128$	-13.4972	-4.2372	2.2743	5.4578	7.9316	9.7548	11.3160	12.6290	13.7356
$K = 256$	-25.1622	-17.8270	-10.6694	-5.7151	-1.2017	2.6200	5.1869	7.0659	8.7133
$K = 512$	-33.8273	-29.5091	-23.3246	-17.6190	-15.4697	-10.4416	-7.9380	-5.7282	-2.7758
$K = 1024$	-40.9693	-36.2091	-30.4133	-30.6181	-27.3662	-24.1144	-20.3935	-17.2538	-14.1951

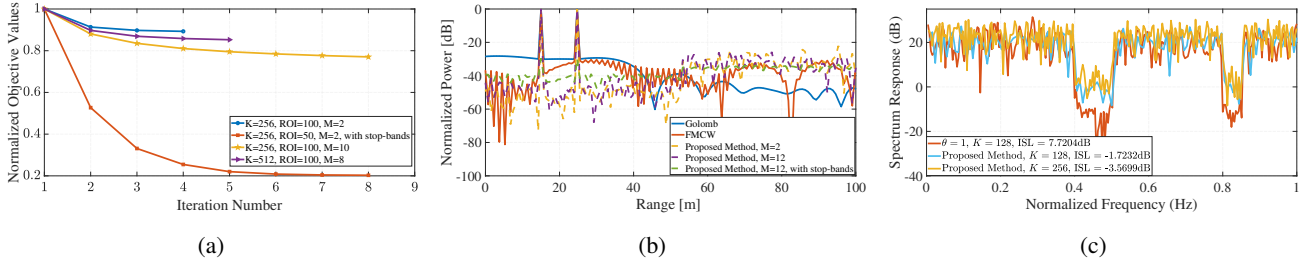


Fig. 2. (a) objective values, (b) Range profiles, and (c) Spectrum of the proposed method for different code lengths compared to [27]

transmit waveforms, and proposed an entry-based optimization method to design transmit sequences with near perfect orthogonality in terms of correlation sidelobes in the required ROI and spectrum shaping with defining an unconstrained optimization problem. The numerical examples and simulation results show that our proposed method can achieve a good performance in mmWave 4D-imaging radar sensors.

REFERENCES

- [1] M. Stolz, M. Wolf, F. Meinel, M. Kunert, and W. Menzel, "A new antenna array and signal processing concept for an automotive 4D radar," in *2018 15th European Radar Conference (EuRAD)*, 2018, pp. 63–66.
- [2] R. Amar, M. Alae-Kerahroodi, P. Babu, and B. S. M. R., "Designing interference-immune doppler-tolerant waveforms for radar systems," *IEEE Trans. on Aerospace and Electronic Systems*, pp. 1–20, 2022.
- [3] M. Alae-Kerahroodi, A. Aubry, A. De Maio, M. M. Naghsh, and M. Modarres-Hashemi, "A coordinate-descent framework to design low PSL/ISL sequences," *IEEE Trans. Signal Process.*, vol. 65, no. 22, pp. 5942–5956, Nov. 2017.
- [4] M. Alae-Kerahroodi, M. Modarres-Hashemi, and M. M. Naghsh, "Designing sets of binary sequences for mimo radar systems," *IEEE Trans. Signal Process.*, vol. 67, no. 13, pp. 3347–3360, July 2019.
- [5] E. Raei, M. Alae-Kerahroodi, P. Babu, and M. R. B. Shankar, "Design of MIMO radar waveforms based on lp-norm criteria," 2021.
- [6] E. Raei, M. Alae-Kerahroodi, and M. B. Shankar, "Spatial- and range-islr trade-off in mimo radar via waveform correlation optimization," *IEEE Transactions on Signal Processing*, vol. 69, pp. 3283–3298, 2021.
- [7] Y. Sun, M. Bauduin, and A. Bourdoux, "Enhancing Unambiguous velocity in Doppler-Division Multiplexing MIMO radar," in *2021 18th European Radar Conference (EuRAD)*, 2022, pp. 493–496.
- [8] J. Jung, S. Lim, S.-C. Kim, and S. Lee, "Solving Doppler-Angle Ambiguity of BPSK-MIMO FMCW Radar system," *IEEE Access*, vol. 9, pp. 120 347–120 357, 2021.
- [9] A. B. Baral and M. Torlak, "Joint Doppler Frequency and Direction of Arrival Estimation for TDM MIMO Automotive Radars," *IEEE Journal of Selected Topics in Signal Processing*, vol. 15, pp. 980–995, 2021.
- [10] R. Feger, C. Pfeffer, and A. Stelzer, "A Frequency-Division MIMO FMCW Radar System Based on Delta-Sigma Modulated Transmitters," *IEEE Transactions on Microwave Theory and Techniques*, vol. 62, no. 12, pp. 3572–3581, 2014.
- [11] F. Xu, S. A. Vorobyov, and F. Yang, "Transmit Beamspace DDMA Based Automotive MIMO Radar," *IEEE Trans. Veh. Technol.*, vol. 71, no. 2, pp. 1669–1684, 2022.
- [12] O. Bialer, A. Jonas, and T. Tirer, "Code optimization for fast chirp FMCW automotive MIMO radar," *IEEE Trans. Veh. Technol.*, vol. 70, no. 8, pp. 7582–7593, 2021.
- [13] F. Yang, F. Xu, X. Yang, and Q. Liu, "DDMA MIMO radar system for low, slow, and small target detection," *The Journal of Engineering*, vol. 2019, no. 19, pp. 5932–5935, 2019.
- [14] M. Q. Nguyen, R. Feger, J. Bechter, M. Pichler-Scheder, M. H. Hahn, and A. Stelzer, "Fast-Chirp FDMA MIMO Radar System Using Range-Division Multiple-Access and Doppler-Division Multiple-Access," *IEEE Transactions on Microwave Theory and Techniques*, vol. 69, no. 1, pp. 1136–1148, 2021.
- [15] R. Amar, M. Alae-Kerahroodi, and M. R. Bhavani Shankar, "FMCW-FMCW interference analysis in mm-wave radars; an indoor case study and validation by measurements," in *2021 21st International Radar Symposium (IRS)*, 2021, pp. 1–11.
- [16] H. He, P. Stoica, and J. Li, "Designing unimodular sequence sets with good correlations; including an application to MIMO radar," *IEEE Trans. Signal Process.*, vol. 57, no. 11, pp. 4391–4405, Nov. 2009.
- [17] G. Cui, X. Yu, M. Piezzo, and L. Kong, "Constant modulus sequence set design with good correlation properties," *Signal Processing*, vol. 139, pp. 75–85, 2017.
- [18] Y. Li and S. A. Vorobyov, "Fast algorithms for designing unimodular waveform(s) with good correlation properties," *IEEE Trans. Signal Process.*, vol. 66, no. 5, pp. 1197–1212, Mar. 2018.
- [19] J. Song, P. Babu, and D. P. Palomar, "Sequence set design with good correlation properties via majorization-minimization," *IEEE Trans. Signal Process.*, vol. 64, no. 11, pp. 2866–2879, June 2016.
- [20] M. Alae-Kerahroodi, M. R. Bhavani Shankar, K. V. Mishra, and B. Ottersten, "Meeting the lower bound on designing set of unimodular sequences with small aperiodic/periodic islr," in *2019 20th International Radar Symposium (IRS)*, 2019, pp. 1–13.

- [21] E. Raei, M. Alae-Kerahroodi, P. Babu, and M. Bhavani Shankar, "Generalized waveform design for sidelobe reduction in mimo radar systems," *Signal Processing*, vol. 206, p. 108914, 2023. [Online]. Available: <https://www.sciencedirect.com/science/article/pii/S0165168422004534>
- [22] Z. Cheng, Z. He, M. Fang, J. Li, and J. Xie, "Spectrally compatible waveform design for MIMO radar transmit beampattern with PAR and similarity constraints," in *2018 IEEE International Conference on Acoustics, Speech and Signal Processing (ICASSP)*, 2018, pp. 3286–3290.
- [23] M. Alae-Kerahroodi, K. V. Mishra, M. R. Bhavani Shankar, and B. Ottersten, "Discrete-phase sequence design for coexistence of MIMO radar and MIMO communications," in *2019 IEEE 20th International Workshop on Signal Processing Advances in Wireless Communications (SPAWC)*, 2019, pp. 1–5.
- [24] S. Shi, Z. Wang, Z. He, and Z. Cheng, "Spectrally compatible waveform design for MIMO radar with ISL and PAPR constraints," *IEEE Sensors Journal*, vol. 20, no. 5, pp. 2368–2377, 2020.
- [25] L. Zheng, M. Lops, Y. C. Eldar, and X. Wang, "Radar and communication coexistence: An overview: A review of recent methods," *IEEE Signal Processing Magazine*, vol. 36, no. 5, pp. 85–99, 2019.
- [26] E. Raei, M. Alae-Kerahroodi, and B. S. M. R. Rao, "Waveform design for Range-ISL minimization with spectral compatibility in MIMO radars," in *2022 19th European Radar Conference (EuRAD)*, 2022, pp. 101–104.
- [27] M. Alae-Kerahroodi, E. Raei, S. Kumar, and B. S. M. R. R. R., "Cognitive radar waveform design and prototype for coexistence with communications," *IEEE Sensors Journal*, pp. 1–1, 2022.